

Effects of Neutrino Inverse Seesaw Mechanism on the Sparticle Spectrum in CMSSM and NUHM2

I. Gogoladze^{a,1}, B. He^{a,2}, A. Mustafayev^{b,3}, S. Raza^{c,4} and Q. Shafi^{a,5}

^a *Bartol Research Institute, Department of Physics and Astronomy, University of Delaware, Newark, DE 19716, USA*

^b *Department of Physics and Astronomy, University of Hawaii, Honolulu, HI 96822, USA*

^c *State Key Laboratory of Theoretical Physics and Kavli Institute for Theoretical Physics China (KITPC), Institute of Theoretical Physics, Chinese Academy of Sciences, Beijing 100190, P. R. China*

Abstract

We study the implications of the inverse seesaw mechanism (ISS) on the sparticle spectrum in the Constrained Minimal Supersymmetric Standard Model (CMSSM) and Non-Universal Higgs Model (NUHM2). Employing the maximal value of the Dirac Yukawa coupling involving the up type Higgs doublet provides a 2-3 GeV enhancement of the lightest CP-even Higgs boson mass. This effect permits one to have lighter colored sparticles in the CMSSM and NUHM2 scenarios with LSP neutralino, which can be tested at LHC14. We present a variety of LHC testable benchmark points with the desired LSP neutralino dark matter relic abundance.

¹E-mail:ilia@bartol.udel.edu

² E-mail:hebin@udel.edu

³ E-mail:azar@phys.hawaii.edu

⁴ E-mail:shabbar@itp.ac.cn

⁵ E-mail:shafi@bartol.udel.edu

1 Introduction

The recent discovery of the Standard Model (SM)-like Higgs boson with mass $m_h = 125.5 \pm 0.5$ GeV by the ATLAS [1] and CMS [2] experiments at the Large Hadron Collider (LHC) has sparked detailed examinations of viable regions of the parameter space of low scale supersymmetry. This is largely motivated by the fact that the Minimal Supersymmetric Standard Model (MSSM) predicts an upper bound on the mass of the lightest CP-even Higgs boson mass, $m_h \lesssim 135$ GeV [3]. The Higgs boson mass and the corresponding sparticle spectrum strongly depend on the soft supersymmetry breaking (SSB) parameters [4], which can be tested at the LHC (see, for instance [5, 6, 7]).

In low scale supersymmetry, a Higgs boson mass of around 125 GeV requires either a relatively large value, $\mathcal{O}(\text{few} - 10)$ TeV, for the geometric mean of top squark masses [6], or a large SSB trilinear A_t -term, with a geometric mean of the top squark masses of around a TeV [7]. The presence of heavy top squarks typically yields a heavy sparticle spectrum in gravity mediated supersymmetry breaking [8], if universality at M_{GUT} of sfermion masses is assumed. It is especially hard in this case to achieve colored sparticles lighter than 2.5 TeV.

The current LHC lower bounds on the colored sparticle masses from LHC data are $m_{\tilde{g}} \gtrsim 1.5$ TeV (for $m_{\tilde{g}} \sim m_{\tilde{q}}$), and $m_{\tilde{g}} \gtrsim 0.9$ TeV (for $m_{\tilde{g}} \ll m_{\tilde{q}}$) [9, 10], and it is expected that the LHC14 can test squarks and gluinos with masses up to 3.5 TeV [11]. In order to be able to reduce the sparticle masses to more accessible values in models with universal sfermion and gaugino masses, we require additional contributions from new physics, which preserves gauge coupling unification.

Solar and atmospheric neutrino oscillation experiments have established that at least two neutrino states are massive [12]. On the theoretical side the nature of the physics responsible for neutrino masses and flavor properties remains largely unknown and is a subject of extensive investigations [13]. Since our goal is to lower the sparticle mass spectrum while preserving gauge coupling unification, we utilize in this paper the inverse seesaw mechanism (ISS) for generating the light neutrino masses [14]. Introducing only SM singlet fields allows one to realize the ISS mechanism, and all new fields can be below the TeV scale. In addition, we can have $\mathcal{O}(1)$ Dirac Yukawa couplings involving the up type Higgs doublet. It has been shown in Refs. [15, 16] that the Dirac Yukawa coupling can impact the lightest CP-even Higgs boson mass through radiative corrections and increase it by 2-3 GeV when the additional new fields are SM singlets. The ISS mechanism can also be realized using $SU(2)_W$ weak triplets [15], and in this case the Higgs mass can be enhanced by more than 10 GeV.

In this paper we restrict ourselves to the case of SM singlet fields since we do not want to disturb gauge coupling unification. An enhancement by 2-3 GeV of the CP-even SM-like Higgs boson mass, as we will show, can yield significant reductions of sparticle masses in the Constrained Minimal Supersymmetric Standard Model (CMSSM) [8] and Non-Universal Higgs Model with $m_{H_u}^2 \neq m_{H_d}^2$ (NUHM2) [17]. Here $m_{H_u}^2$ and $m_{H_d}^2$ denote the SSB mass square terms for the up and down type MSSM Higgs doublets respectively.

The outline for the rest of the paper is as follows. In section 2 we briefly describe the model including the SSB parameters, the range of values employed in our scan, and the scanning procedure. The relevant experimental constraints that we have employed are described in section 3. The results pertaining to CMSSM, CMSSM-ISS and NUHM2-ISS are discussed in

section 4, and our conclusions are summarized in section 5.

2 Inverse Seesaw Mechanism and Higgs Boson Mass

In order to explain non-zero neutrino masses and mixings by the ISS mechanism [14], we supplement the MSSM field content with three pairs of MSSM singlet chiral superfields ($N_i^c + N_i$), $i = 1, 2, 3$, and a singlet chiral superfield S which develops a vacuum expectation value (VEV) comparable to or less than the electroweak scale. The part of the renormalizable superpotential involving only the new chiral superfields is given by

$$W \supset Y_{N_{ij}} N_i^c H_u L_j + \lambda_{N_{ij}} S N_i N_j + m_{ij} N_i^c N_j. \quad (1)$$

Here $Y_{N_{ij}}$ and $\lambda_{N_{ij}}$ are dimensionless couplings and m_{ij} is a mass term. A non-zero VEV for the scalar component of S generates the lepton-number-violating term $\mu_s N_i N_j \equiv \lambda_{N_{ij}} \langle S \rangle N_i N_j$ and, as a result, Majorana masses for the observed neutrinos can be generated. The coupling $\lambda_{N_{ij}} S N_i N_j$ is preferred over the direct mass term $\mu N_i N_j$, with the former yielding the desired mass terms for the N fields with a non-zero $\langle S \rangle$. A singlet chiral superfield S can make it easier to find extension of the SM gauge group with help from a suitable symmetry (see, for instance, Refs. [15, 18]), and avoid terms which otherwise may spoil the ISS mechanism.

The SSB terms pertaining to the fields N_i^c and N_i are given by

$$\mathcal{L}^{\text{soft}} \supset m_{N_c}^2 \widetilde{N}^{c\dagger} \widetilde{N}^c + m_N^2 \widetilde{N}^\dagger \widetilde{N} + \left[A_\nu^{ij} \widetilde{L}_i \widetilde{N}^c_j H_u + B_m^{jk} \widetilde{N}^c_j \widetilde{N}_k + B_{\mu_N}^{jk} \widetilde{N}_j \widetilde{N}_k + \text{h.c.} \right], \quad (2)$$

where the SSB parameters are prescribed at the TeV SUSY breaking scale. In the ISS case there are regions of the SSB parameter space for which one of the sneutrinos can be the lightest supersymmetric particle (LSP). The phenomenology of models of this kind has been studied in Ref. [18]. In our present work we assume that the lightest neutralino is the LSP, and a spectrum of this nature can be realized both in the CMSSM and NUHM2 if we assume that all sfermions, including the N_i^c and N_i fields, have universal SSB mass terms at M_{GUT} .

According to the superpotential in Eq. (1), after integrating out the ($N_i^c + N_i$) fields, the neutrino mass arises from the effective dimension six operator (Figure. 1):

$$\frac{LLH_u H_u S}{M_6^2}. \quad (3)$$

We assume here that $M_6 \delta_{ij} \equiv m_{ij}$ is larger than the electroweak scale. Also, in Eq. (3) the family and $SU(2)_W$ gauge indices are omitted.

Following the electroweak symmetry breaking, the neutrino Majorana mass matrix is generated:

$$m_\nu = \frac{(Y_N^T Y_N) v_u^2}{M_6} \times \frac{\lambda_N \langle S \rangle}{M_6}. \quad (4)$$

For simplicity, we set $Y_N \equiv Y_{N_{ij}}$ and $\lambda_N \equiv \lambda_{N_{ij}}$, and v_u , $\langle S \rangle$ are the VEVs of H_u , and the S field. Eq. (4) implies that even if we require $Y_N \sim \mathcal{O}(1)$ and $M_6 \sim 1$ TeV, the correct mass scale for the light neutrinos can be reproduced by suitably adjusting $\lambda_N \langle S \rangle$.

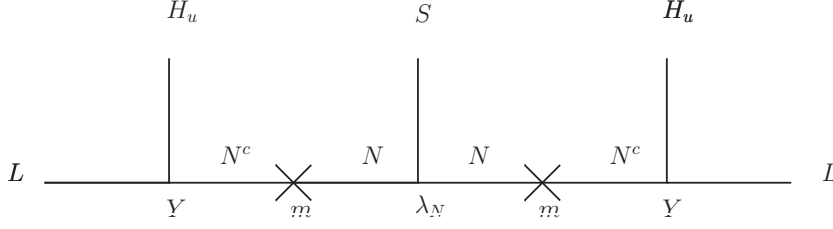


Figure 1: Supergraph leading to dimension six operator for neutrino masses .

Keeping $Y_N \sim \mathcal{O}(1)$ will provide sizable contribution to the lightest CP-even Higgs mass, which is given by [19]

$$[m_h^2]_N = n \times \left[-M_Z^2 \cos^2 2\beta \left(\frac{1}{8\pi^2} Y_N^2 t_N \right) + \frac{1}{4\pi^2} Y_N^4 v^2 \sin^4 \beta \left(\frac{1}{2} \tilde{X}_{Y_N} + t_N \right) \right], \quad (5)$$

where

$$t_N = \log \left(\frac{M_S^2 + M_6^2}{M_6^2} \right), \quad \tilde{X}_{Y_N} = \frac{4\tilde{A}_{Y_N}^2 (3M_S^2 + 2M_6^2) - \tilde{A}_{Y_N}^4 - 8M_S^2 M_6^2 - 10M_S^4}{6(M_S^2 + M_6^2)^2}, \quad (6)$$

and

$$\tilde{A}_{Y_N} = A_{Y_N} - Y_N \langle S \rangle \cot \beta. \quad (7)$$

Also, $A_{Y_N} \equiv A_{\nu}^{ij}$ is the SSB mixing parameter in Eq. (2), n is the number of pairs of new MSSM singlets, $M_S = \sqrt{m_{\tilde{t}_L} m_{\tilde{t}_R}}$ defines the SUSY scale, and $v = 174.1$ GeV is the electroweak VEV.

We incorporate the ISS mechanism in CMSSM and NUHM2 and scan the SUSY parameter space using the ISAJET 7.84 package [20]. We modify the code by including the additional contributions from Eq. (5) to the lightest CP-even Higgs boson mass.

3 Phenomenological constraints and scanning procedure

We employ the ISAJET 7.84 package [20] to generate sparticle spectrum over the fundamental parameter space. In this package, the weak scale values of the gauge, third generation Yukawa couplings, including the Yukawa coupling $N_i^c H_u L_j$ from ISS, are evolved to M_{GUT} via the MSSM renormalization group equations (RGEs) in the \overline{DR} regularization scheme. With the boundary conditions given at M_{GUT} , all of the SSB parameters, along with the gauge and Yukawa couplings, are evolved back to the weak scale M_Z . The data points collected all satisfy the requirement of radiative electroweak symmetry breaking condition with the neutralino in each case being the LSP.

We have performed Markov-chain Monte Carlo (MCMC) scans for the following CMSSM

parameter range:

$$\begin{aligned}
0 &\leq m_0 \leq 10 \text{ TeV}, \\
0 &\leq m_{1/2} \leq 5 \text{ TeV}, \\
-3 &\leq A_0/m_0 \leq 3, \\
3 &\leq \tan \beta \leq 60,
\end{aligned} \tag{8}$$

with $\mu > 0$ and $m_t = 173.3 \text{ GeV}$ [21]. We use $m_b^{\overline{DR}}(M_Z) = 2.83 \text{ GeV}$ which is hard-coded into ISAJET. Here m_0 is the universal SSB mass parameter for MSSM sfermions, Higgs and additional N^c , N and S fields. $m_{1/2}$ is the gaugino mass parameter, $\tan \beta$ is the ratio of the VEVs of the two MSSM Higgs doublets, and A_0 is the MSSM universal SSB trilinear scalar coupling. In order to maximize the contribution from the ISS mechanism to the Higgs boson mass, we set $\tilde{X}_{Y_N} = 4$, following Ref. [15].

In the case of NUHM2, in addition to the above mentioned parameters we have two additional independent SSM mass parameters m_{H_d} and m_{H_u} . We use the following parameter range for them:

$$\begin{aligned}
0 &\leq m_{H_u} \leq 10 \text{ TeV}, \\
0 &\leq m_{H_d} \leq 10 \text{ TeV}.
\end{aligned} \tag{9}$$

To maximize the impact of ISS on the sparticle spectrum, we set $\lambda_N = 0.7$. This is the maximal value of λ_N at low scale that remains perturbative up to M_{GUT} . We also assume that M_6 is larger than M_S , in order that the neutralino rather than sneutrino is the LSP.

After collecting the data, we impose the mass bounds on all the particles [22] and use the IsaTools package [23] and Ref. [24] to implement the following phenomenological constraints:

$$m_h = 123 - 127 \text{ GeV} \quad [25, 26] \tag{10}$$

$$0.8 \times 10^{-9} \leq \text{BR}(B_s \rightarrow \mu^+ \mu^-) \leq 6.2 \times 10^{-9} \text{ (} 2\sigma \text{)} \quad [27] \tag{11}$$

$$2.99 \times 10^{-4} \leq \text{BR}(b \rightarrow s \gamma) \leq 3.87 \times 10^{-4} \text{ (} 2\sigma \text{)} \quad [28] \tag{12}$$

$$0.15 \leq \frac{\text{BR}(B_u \rightarrow \tau \nu_\tau)_{\text{MSSM}}}{\text{BR}(B_u \rightarrow \tau \nu_\tau)_{\text{SM}}} \leq 2.41 \text{ (} 3\sigma \text{)} \quad [29] \quad . \tag{13}$$

As far as the muon anomalous magnetic moment a_μ is concerned, we require that the benchmark points are at least as consistent with the data as the SM.

For the benchmark points presented in Table 1 and 2, we require that the LSP neutralino dark matter abundance lies in the interval $0.0913 \leq \Omega_{\text{CDM}} h^2 \leq 0.1363$ [30].

Finally we implement the following following bounds on the sparticle masses:

$$m_{\tilde{g}} \gtrsim 1.5 \text{ TeV (for } m_{\tilde{g}} \sim m_{\tilde{q}} \text{)} \quad \text{and} \quad m_{\tilde{g}} \gtrsim 0.9 \text{ TeV (for } m_{\tilde{g}} \ll m_{\tilde{q}} \text{)} \quad [9, 10]. \tag{14}$$

4 Results

4.1 CMSSM and Inverse Seesaw

In this section we present our results for the CMSSM and the CMSSM with additional ISS contribution (CMSSM-ISS). The main idea behind the presentation of these results is to show that

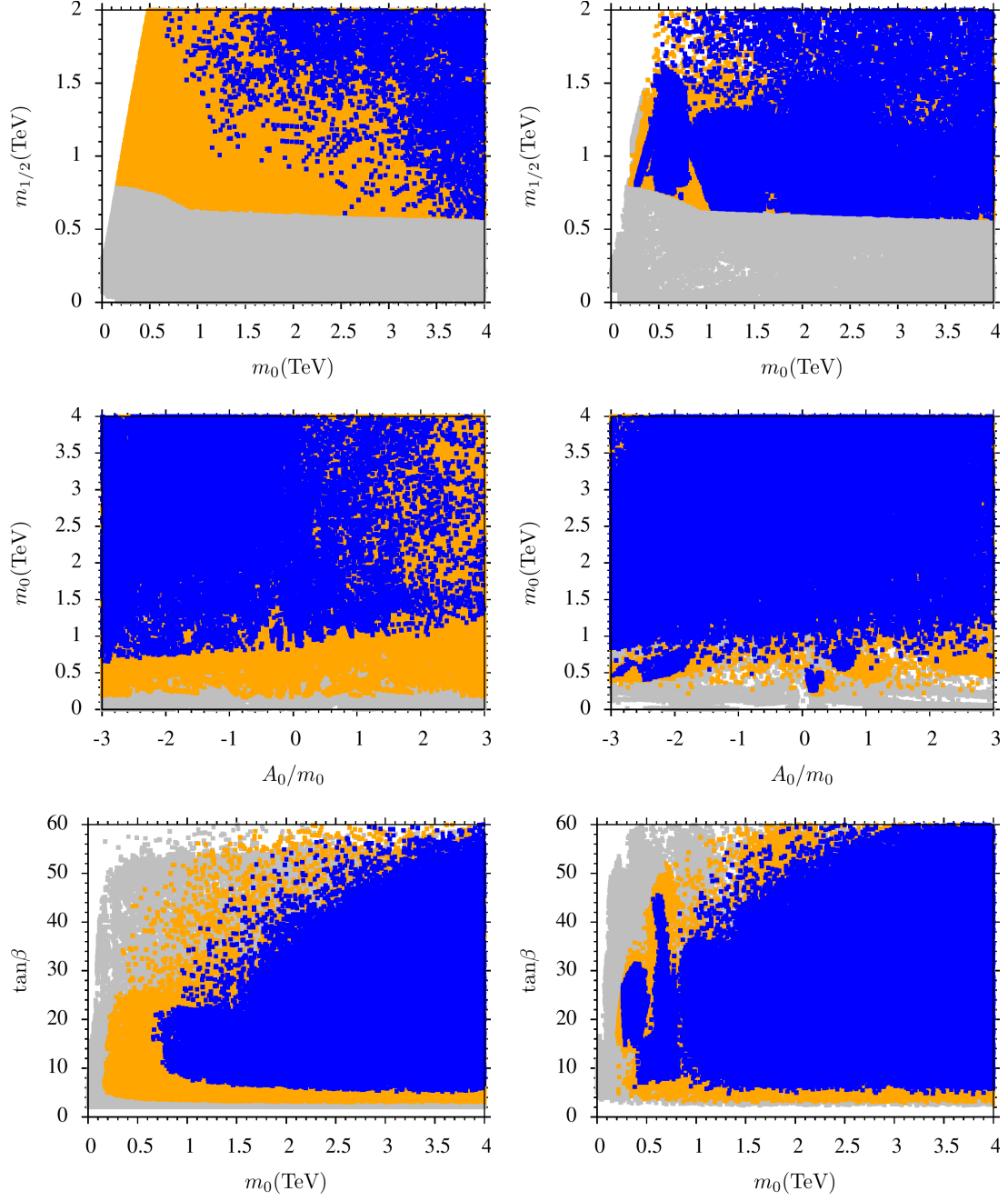


Figure 2: Plots in $m_0 - m_{1/2}$, $A_0/m_0 - m_0$ and $m_0 - \tan\beta$ planes for CMSSM (left panel) and CMSSM-ISS (right panel). Grey points satisfy REWSB and LSP neutralino conditions. Orange point solutions satisfy mass bounds and B-physics bounds given in Section 2. Points in blue are a subset of orange points and satisfy $123 \text{ GeV} \lesssim m_h \lesssim 127 \text{ GeV}$.

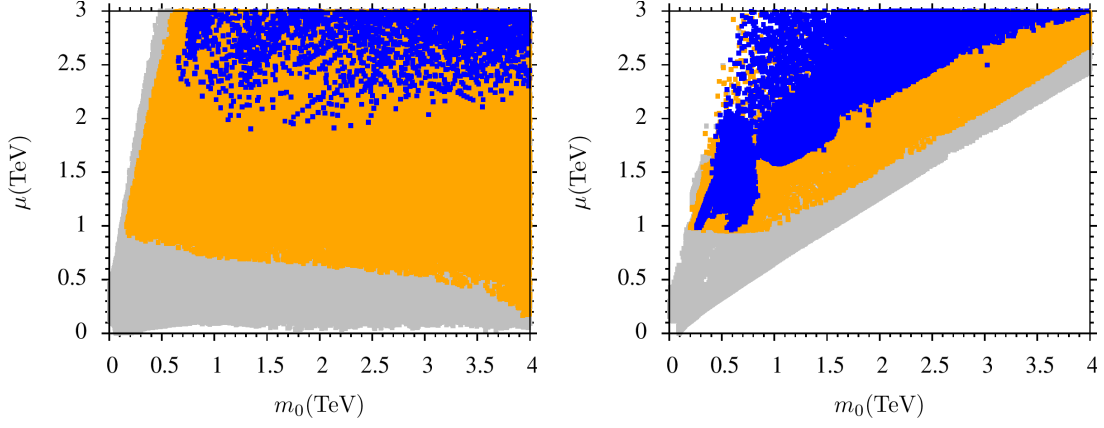


Figure 3: Plots in $m_0 - \mu$ plane for CMSSM (left panel) and CMSSM-ISS (right panel). Color coding is the same as in Figure 2.

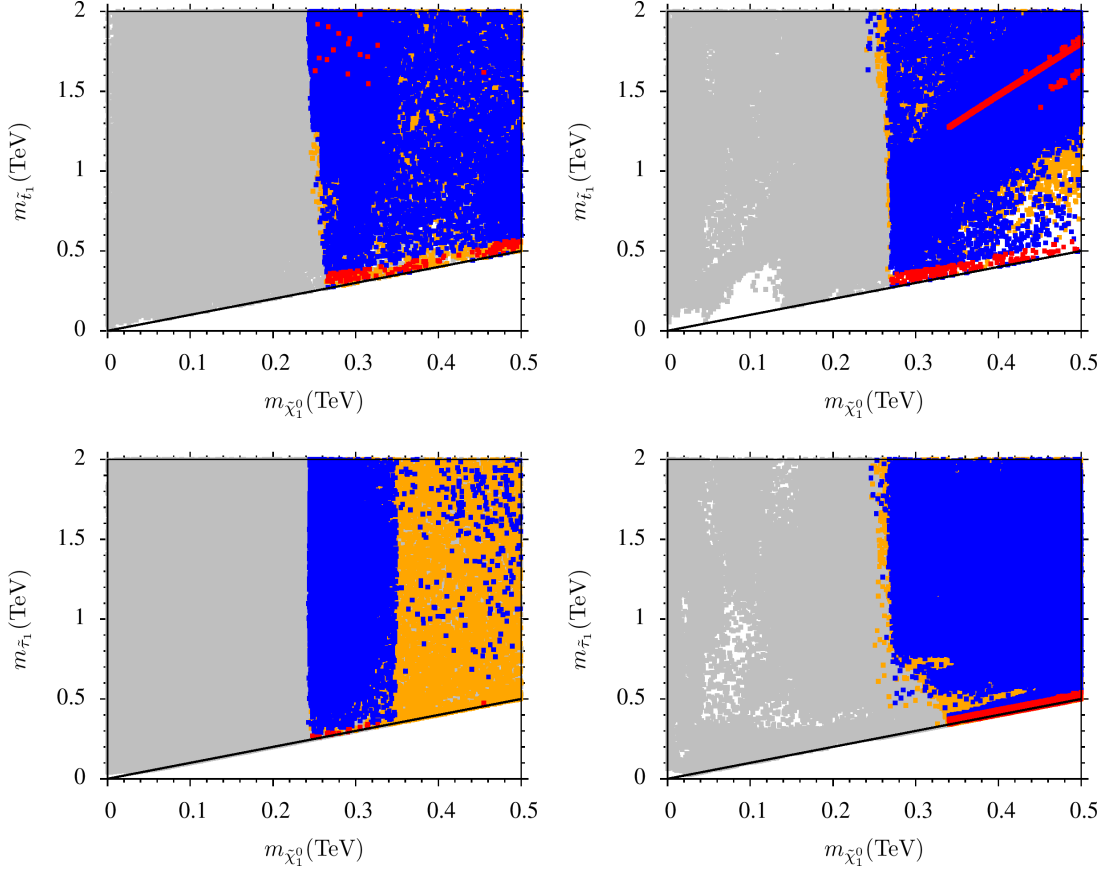


Figure 4: Plots in $m_{\tilde{\chi}_1^0} - m_{\tilde{t}_1}$ and $m_{\tilde{\chi}_1^0} - m_{\tilde{\tau}_1}$ planes for CMSSM (left panel) and CMSSM-ISS (right panel). The color coding is the same as in Figure 2 except that red points are a subset of blue point solutions and also satisfy bounds for relic abundance, $0.001 \leq \Omega h^2 \leq 1$.

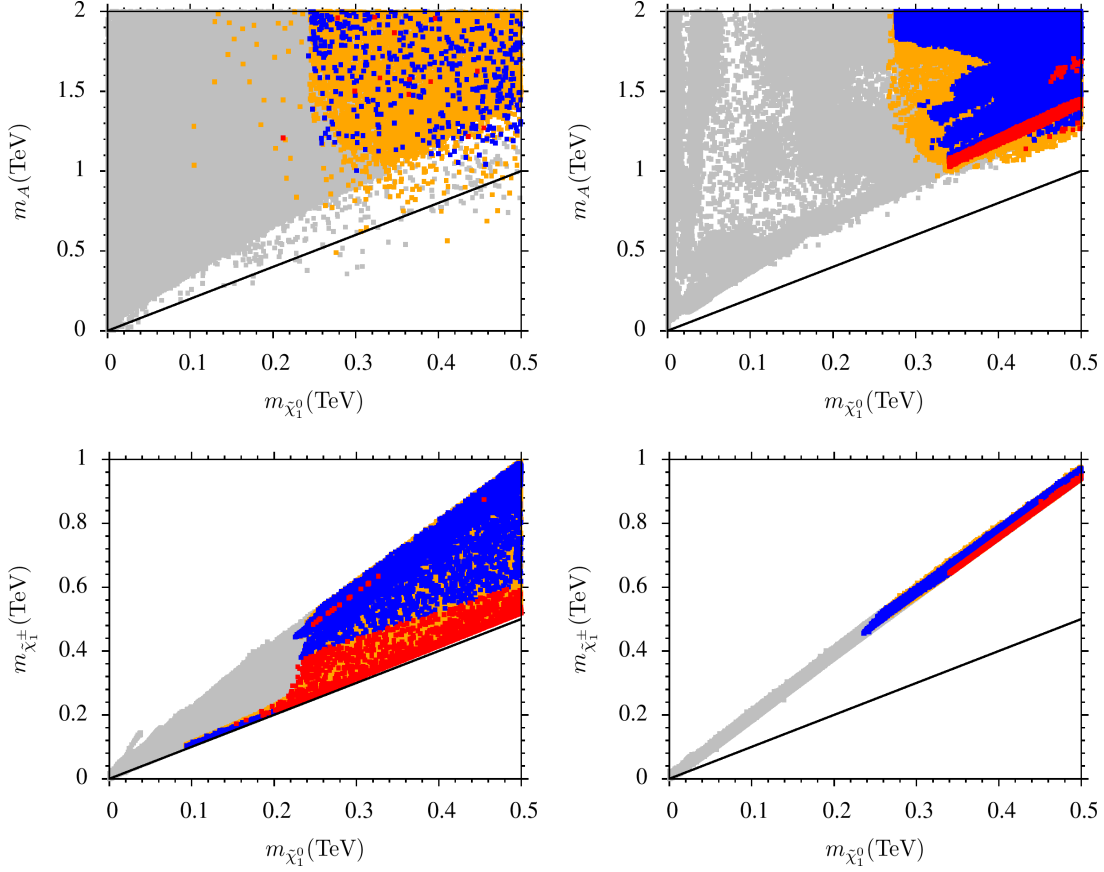


Figure 5: Plots in $m_{\tilde{\chi}_1^0} - m_A$ and $m_{\tilde{\chi}_1^0} - m_{\tilde{\chi}_1^\pm}$ planes for CMSSM (left panel) and CMSSM-ISS (right panel). The color coding is the same as in Figure 2 except that red points are subset of blue point solutions and also satisfy bounds for relic abundance, $0.001 \leq \Omega h^2 \leq 1$.

these two scenarios have quite distinct features as far as choice for the fundamental parameters of the models is concerned. In Figure 2, the left panels represent our results for the CMSSM, while the right panels display our results for the CMSSM-ISS. Here grey points satisfy REWSB and the LSP neutralino requirement. The orange points represent solutions which satisfy the mass bounds and B-physics bounds from Section 3. Solutions in blue color are a subset of orange points and satisfy the requirement $123 \text{ GeV} \lesssim m_h \lesssim 127 \text{ GeV}$. This figure clearly serves our purpose stated above.

For instance, the graph in $m_0 - m_{1/2}$ plane shows that for the CMSSM case, the Higgs mass bounds excludes simultaneously small values for m_0 and $m_{1/2}$, while in the CMSSM-ISS case, we can have relatively small values for $m_{1/2}$ ($< 800 \text{ GeV}$) and m_0 ($< 400 \text{ GeV}$), consistent with all constraints given in section 3. There is also noticeable difference between CMSSM and CMSSM-ISS in the $A_0/m_0 - m_0$ plane. In the CMSSM case, for instance, we find $m_0 \sim 700 \text{ GeV}$ for $A_0/m_0 = -3$, and for $A_0/m_0 = 3$ we have $m_0 \sim 1.3 \text{ TeV}$. In CMSSM-ISS, on the other hand, the corresponding minimum m_0 values vary from 400 GeV to 1.1 TeV . In the $m_0 - \tan \beta$ plane too, considering the blue points, we see in the left panel that for a minimum value $m_0 \sim 700 \text{ GeV}$, the corresponding $\tan \beta$ value is around 16. In the right panel, on the

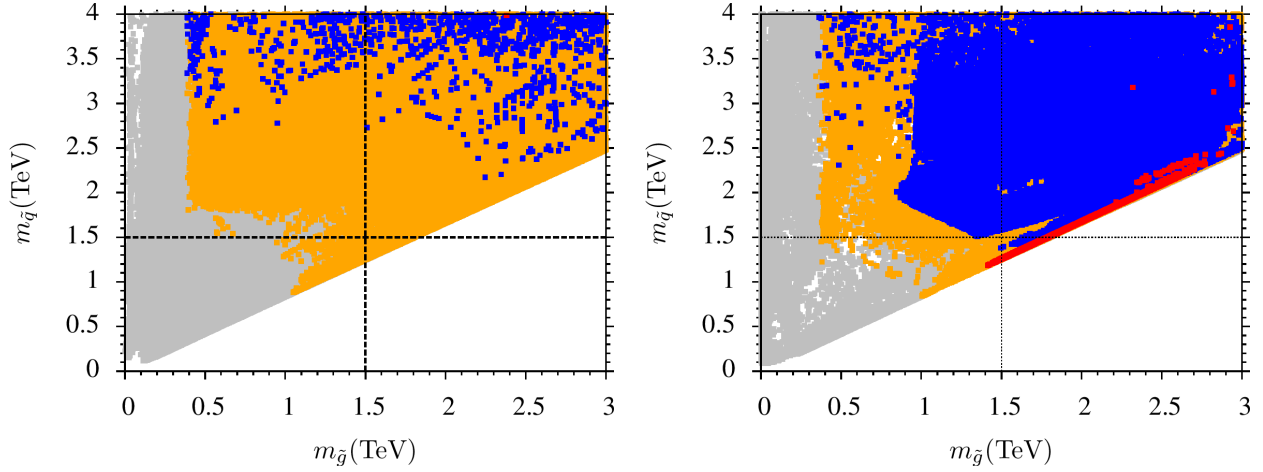


Figure 6: Plots in $m_{\tilde{g}} - m_{\tilde{q}}$ planes for CMSSM (left panel) and CMSSM-ISS (right panel). The color coding is the same as in Figure 2, except that orange points do not satisfy mass bounds for gluinos and first two generation squarks, and red points are a subset of blue point solutions and also satisfy bounds for relic abundance, $0.001 \leq \Omega h^2 \leq 1$. Dashed vertical and horizontal lines stand for current squark and gluino lower mass bounds respectively.

other hand, $\tan \beta$ is again around 16 but now the minimum value of m_0 is ~ 300 GeV.

In Figure 3 we show plots of m_0 versus μ . The color coding is the same as in Figure 2 with the left and right panels representing CMSSM and CMSSM-ISS respectively. This figure shows very distinct features of the two scenarios. Considering the orange points, in CMSSM-ISS we have solutions with $\mu \gtrsim 1$ TeV, in contrast with the CMSSM, where we have solutions with small, as well as large values of μ . The reason for this difference is that in CMSSM-ISS, $m_{H_u}^2$ gets new contribution from the loop induced by the coupling $N_i^c H_u L_j$ in addition to the top quark loop, which makes μ relatively heavy. Thus, in the CMSSM-ISS case we do not have the so-called focus point/hyperbolic branch scenario [31, 32] while it is still a viable solution in the CMSSM case.

In Figure 4, we show graphs in $m_{\tilde{\chi}_1^0} - m_{\tilde{t}_1}$ and $m_{\tilde{\chi}_1^0} - m_{\tilde{\tau}_1}$ planes. The color coding is the same as in Figure 2, except that the solutions in red are a subset of solutions in blue and also satisfy the relic abundance bound $0.001 \leq \Omega h^2 \leq 1$. These graphs show that despite the fact that there are differences in the space of fundamental parameters, the mass spectrum for $\tilde{\chi}_1^0$, \tilde{t}_1 and $\tilde{\tau}_1$ turn out to be more or less identical.

For instance, in the $m_{\tilde{\chi}_1^0} - m_{\tilde{t}_1}$ plane we see that we have NLSP \tilde{t}_1 in the mass range of $\sim 260 - 500$ GeV in both cases. Similar results were also reported in [33, 34] in the case of b - τ Yukawa coupling unification in CMSSM and $SU(5)$. It was shown in [35, 36] that the region of parameter space with stop-neutralino mass difference of 20% is ruled out for $m_{\tilde{t}_1} \lesssim 140$ GeV. In the $m_{\tilde{\chi}_1^0} - m_{\tilde{\tau}_1}$ plane, we note that NLSP $\tilde{\tau}_1$ has the same mass range in CMSSM and CMSSM-ISS. The reason why we have comparable intervals for $m_{\tilde{t}_1}$ and $m_{\tilde{\tau}_1}$ in CMSSM and CMSSM-ISS is that low values for both sparticle masses are achieved via fine tuning involving the trilinear SSB terms, while the addition of ISS to CMSSM mostly affects the first two generation sparticle masses.

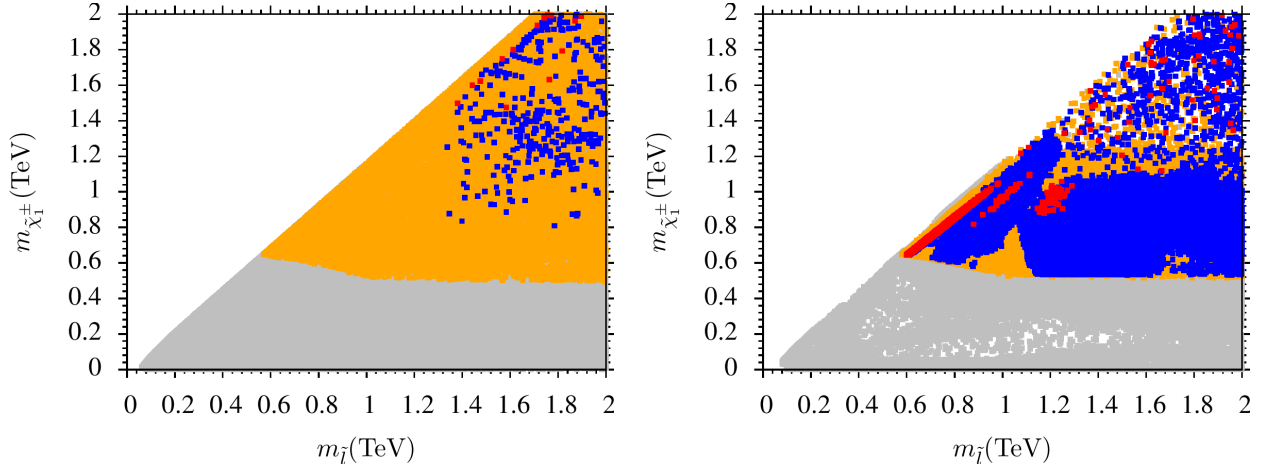


Figure 7: Plots in $m_{\tilde{l}} - m_{\tilde{\chi}_1^\pm}$ planes for CMSSM (left panel) and CMSSM-ISS (right panel). The color coding is the same as in Figure 2, except that red points are a subset of blue point solutions and also satisfy bounds for relic abundance, $0.001 \leq \Omega h^2 \leq 1$.

In Figure 5, we present graphs in $m_{\tilde{\chi}_1^0} - m_A$ and $m_{\tilde{\chi}_1^0} - m_{\tilde{\chi}_1^\pm}$ planes, with color coding the same as in Figure 4. The graphs in $m_{\tilde{\chi}_1^0} - m_A$ plane show that we do not have the A -resonance solution [37], and the reason can be understood from the following equation:

$$m_A^2 = 2|\mu|^2 + m_{H_u}^2 + m_{H_d}^2. \quad (15)$$

In CMSSM, since we have universal scalar masses and we require $m_h \sim 123 - 127$ GeV, $m_{H_u}^2$ and $m_{H_d}^2$ are both large, and, as a result, m_A is also large. This can be seen in the $m_{\tilde{\chi}_1^0} - m_A$ graph in the left panel. The solid black line in the graph represents the condition $2m_{\tilde{\chi}_1^0} = m_A$ for the A -resonance solution [37].

We note that the solutions in orange color lie around the solid black line, but if we apply the constraint $123 \text{ GeV} \lesssim m_h \lesssim 127 \text{ GeV}$, the relevant blue points lie further from the black line. In the right panel, which represents the CMSSM-ISS case, we note that both the orange and blue points are further away from the solid black line. This is because of two reasons. Firstly, as stated earlier, μ is larger because of extra contributions from the $N_i^c H_u L_j$ Yukawa coupling, and so the orange points move away from the solid black line. Secondly, as explained, in the CMSSM case the m_h constraint makes solutions move away from the solid black line as m_A becomes larger.

A more distinctive figure concerning the sparticle spectra in CMSSM and CMSSM-ISS is presented in the $m_{\tilde{\chi}_1^0} - m_{\tilde{\chi}_1^\pm}$ plane. In contrast to CMSSM (left panel), the figure for CMSSM-ISS is quite different. This is due to the fact that in CMSSM-ISS, the LSP neutralino is mostly a bino and the chargino mostly wino. Therefore, the ratio $m_{\tilde{\chi}_1^0}/m_{\tilde{\chi}_1^\pm}$ is close to the ratio of $U(1)$ and $SU(2)$ gauge couplings, $g_1/g_2 \approx 1/2$, and the points form a narrow strip.

In Figure 6 we show $m_{\tilde{q}}$ versus $m_{\tilde{g}}$ for CMSSM (left panel) and CMSSM-ISS (right panel). The color coding is the same as in Figure 2, except that the orange points do not include mass bounds for gluinos and the first two generation squarks. Dashed vertical and horizontal lines represent current squark and gluino mass bounds. We note that especially in the CMSSM

	Point A	Point B
m_0	1020.3	3234
$M_{1/2}$	1091.1	684.6
A_0/m_0	-2.71	-2.97
$\tan \beta$	38	14.4
m_h	125	125
m_H	1602	4744
m_A	1592	4714
m_{H^\pm}	1604	4745
μ	1772	3727
$m_{\tilde{g}}$	2401	1705
$m_{\tilde{\chi}_{1,2}^0}$	476 , 902	312 , 608
$m_{\tilde{\chi}_{3,4}^0}$	1769, 1772	3724, 3724
$m_{\tilde{\chi}_{1,2}^\pm}$	905, 1773	614, 3733
$m_{\tilde{u}_{L,R}}$	2391, 2314	3492, 3476
$m_{\tilde{t}_{1,2}}$	1569, 1983	347 , 2376
$m_{\tilde{d}_{L,R}}$	2392, 2305	3493, 3479
$m_{\tilde{b}_{1,2}}$	1940, 2035	2400, 3262
$m_{\tilde{\nu}_1}$	1248	3265
$m_{\tilde{\nu}_3}$	792	2024
$m_{\tilde{e}_{L,R}}$	1252, 1098	3261, 3245
$m_{\tilde{\tau}_{1,2}}$	497 , 820	2040, 3027
$\sigma_{SI}(\text{pb})$	1.57×10^{-11}	1.71×10^{-15}
$\sigma_{SD}(\text{pb})$	5.05×10^{-9}	7.3×10^{-13}
$\Omega_{CDM} h^2$	0.114	0.092

Table 1: Masses (in GeV units) and other parameters for two CMSSM-ISS benchmark points satisfying all phenomenological constraints discussed in section 3. Points A and B are chosen from the stau-neutralino coannihilation and the stop-neutralino coannihilation regions respectively.

the gluino mass bound excludes a significant portion of the parameter space which otherwise is consistent with the experimental data. The location of blue points relative to the orange points shows how the lower bounds on the squark and gluino masses are pushed up by m_h . It is interesting to observe that there are no red points with neutralino LSP dark matter within the reach of LHC14. Comparing results from $m_{\tilde{g}} - m_{\tilde{q}}$ panel with the results from Figures 4 and 5, we conclude that in the CMSSM, the solution which yields the correct dark matter relic abundance predicts gluino and squarks masses that lie beyond the reach of the LHC14 [11].

On the other hand, comparison of left and right panels in Figure 6 shows the impact of the ISS mechanism on the sparticle masses. We can see from the $m_{\tilde{g}} - m_{\tilde{q}}$ plot in the right panel that plenty of blue points are left after we apply the Higgs mass constraint $123 \text{ GeV} \lesssim m_h \lesssim 127 \text{ GeV}$. This means that in the presence of the ISS mechanism, most points satisfying all experimental constraints lie in the Higgs mass range $123 \text{ GeV} \lesssim m_h \lesssim 127 \text{ GeV}$, which is very

different from the CMSSM case. There are also red points in the right panel which shows that we can have LHC testable solutions with the correct relic abundance of dark matter.

In Figure 7 we display plots for $m_{\tilde{\chi}_1^\pm}$ versus $m_{\tilde{l}}$ in CMSSM (left panel) and CMSSM-ISS (right panel), with the color coding the same as in the previous figures. In the left panel we see from the blue points that $m_{\tilde{l}} > 1.4$ TeV, which may be difficult to test at the LHC. On the other hand, we see in the right panel solutions in blue and red colors around $m_{\tilde{l}} \simeq 500$ GeV, which provides a glimmer of hope that sleptons employing the CMSSM-ISS mechanism may be found at the LHC.

In Table 1 we display two benchmark points for the cMSM-ISS model that are consistent with constraints in Section 3. The LSP neutralino relic density in the two cases is in accord with the WMAP observations, and corresponds to stau-neutralino [38] (stop-neutralino [39]) coannihilation for point A (B). For point A, $m_{\tilde{\tau}_1} \approx 500$ GeV, $m_{\tilde{g}} \approx 2.4$ TeV, the first two generation squarks are close to 2 TeV, while slepton masses are around 1 – 2 TeV. For point B, $m_{\tilde{t}_1} \approx 350$ GeV, $m_{\tilde{g}} \approx 1.7$ TeV, the first two generation squark masses are about 3.4 TeV, while slepton masses are around 3.2 TeV.

4.2 NUHM2 and Inverse Seesaw

In this subsection we present the results of our scan for NUHM2 with ISS contributions (NUHM2-ISS). In Figure 8 we present graphs in $m_0 - m_{1/2}$ and $m_0 - \mu$ planes, with color coding the same as in Figure 2. In the $m_0 - m_{1/2}$ plane we see that the results are similar to what we found in CMSSM-ISS. Again we can have solutions compatible with all experimental constraints presented in section 3. We note that the Higgs mass constraint $123 \text{ GeV} \lesssim m_h \lesssim 127 \text{ GeV}$ provides the lower bounds $m_{1/2} \approx 500$ GeV and $m_0 \approx 1$ TeV. Since μ is a free parameter in NUHM2, we can find solutions with any value of μ compatible with the experimental data (see $m_0 - \mu$ plot). As shown in [40], a relatively small μ term is necessary, but not sufficient, to be consistent with natural supersymmetry (little hierarchy problem) criteria. We find that it is hard to fully resolve the little hierarchy problem in this scenario.

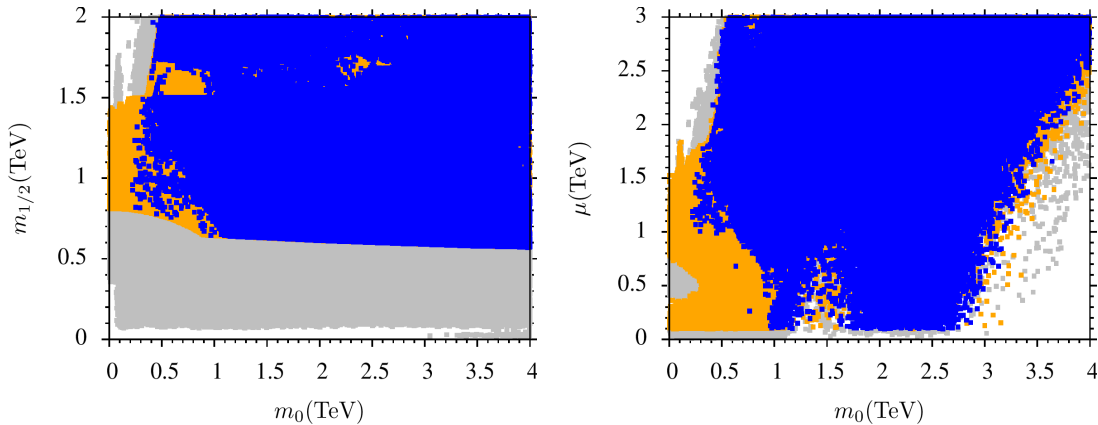


Figure 8: Plots in $m_0 - m_{1/2}$ and $m_0 - \mu$ planes for NUHM2-ISS. The color coding is the same as in Figure 2.

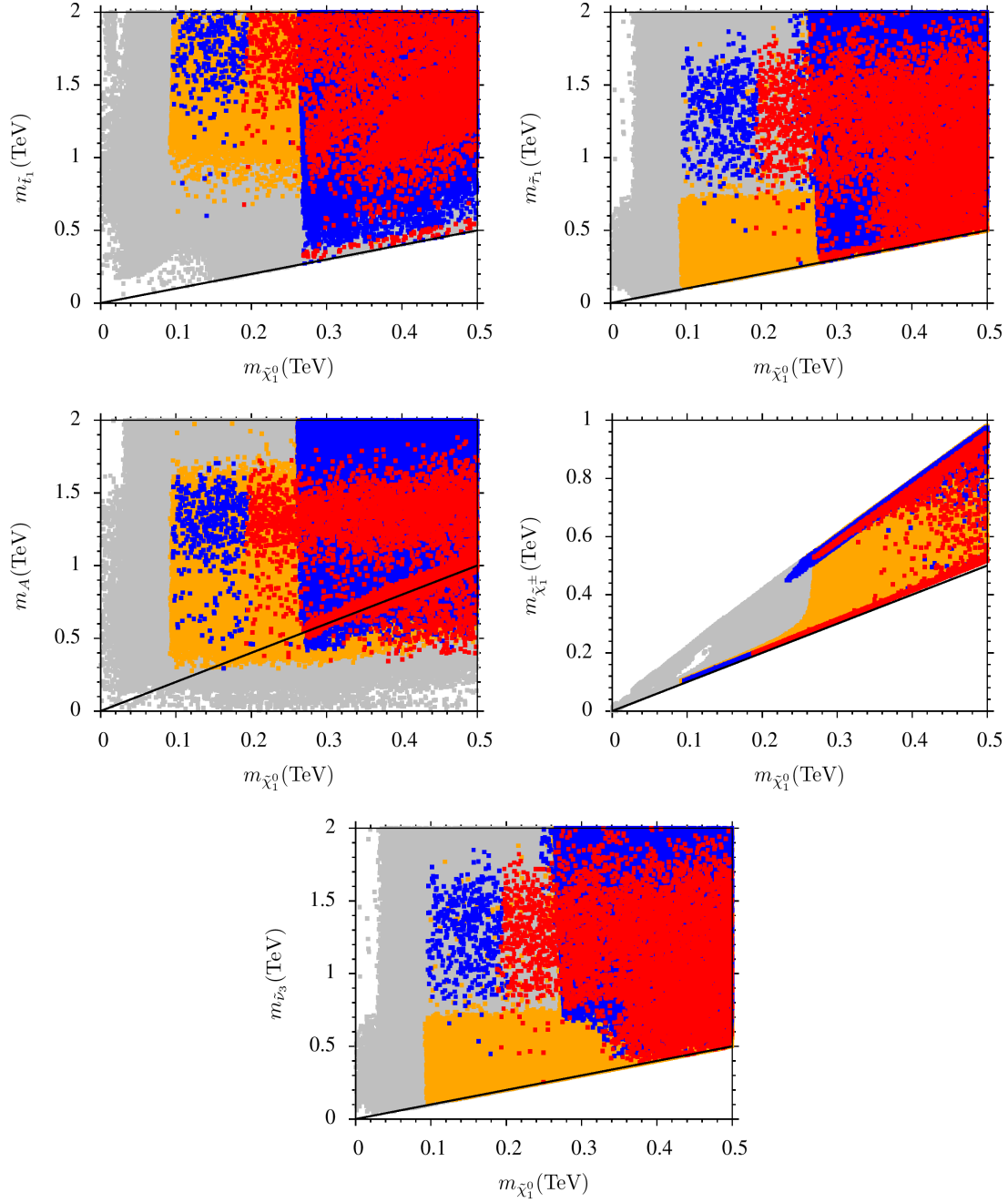


Figure 9: Plots in $m_{\tilde{\chi}_1^0} - m_{\tilde{t}_1}$, $m_{\tilde{\chi}_1^0} - m_{\tilde{\tau}_1}$, $m_{\tilde{\chi}_1^0} - m_A$, $m_{\tilde{\chi}_1^0} - m_{\tilde{\chi}_1^\pm}$ and $m_{\tilde{\chi}_1^0} - m_{\tilde{\nu}_3}$ planes for NUHM2-ISS. The color coding is the same as in Figure 2 except that red points are a subset of blue point solutions and also satisfy bounds for relic abundance, $0.001 \leq \Omega h^2 \leq 1$.

The particle spectrum for NUHM2-ISS is shown in Figure 9, with color coding the same as in the previous figures. The top left panel shows an NLSP \tilde{t}_1 in the mass range of 220 - 500 GeV, which can be tested at LHC14. The top panel on right shows that the NLSP $\tilde{\tau}_1$ can be as light as 250 GeV, which is somewhat lighter than in the CMSSM and CMSSM-ISS scenarios. The

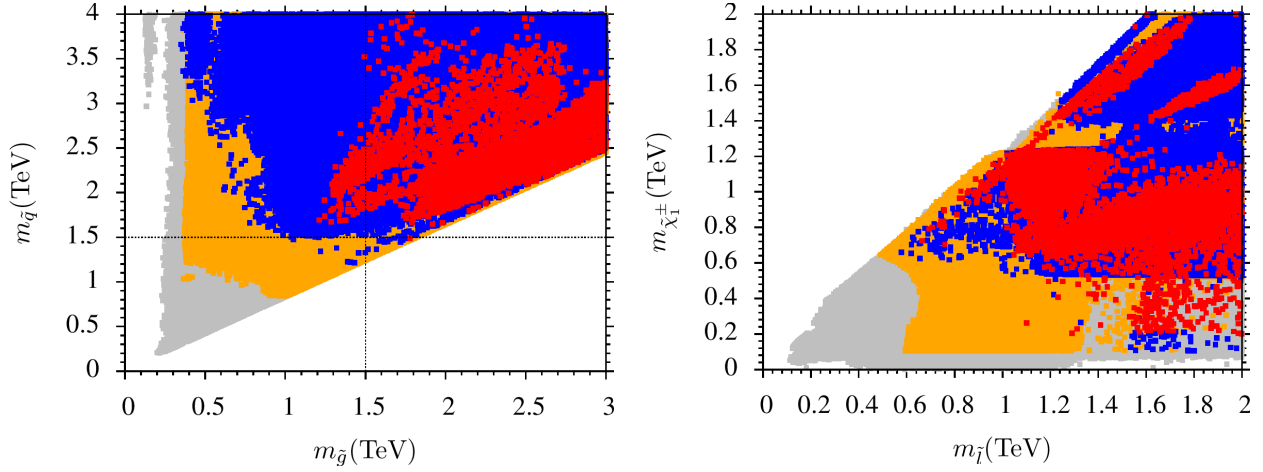


Figure 10: Plots in $m_{\tilde{g}} - m_{\tilde{q}}$ and $m_{\tilde{l}} - m_{\tilde{\chi}_1^\pm}$ planes for NUHM2. In the left panel orange points do not satisfy gluino and first two generation squark mass bounds and red points are a subset of blue point solutions and also satisfy bounds for relic abundance, $0.001 \leq \Omega h^2 \leq 1$. Dashed vertical and horizontal lines stand for current squark and gluino lower mass bounds respectively. Otherwise color coding is the same as in Figure 2.

bottom left panel shows the presence of A -resonance solutions. This follows from the relatively low μ values in NUHM2 (Figure. 8), and with m_{H_u} and m_{H_d} (or equivalently μ and M_A) being independent parameters.

In the bottom right panel we plot $m_{\tilde{\chi}_1^\pm}$ versus $m_{\tilde{\chi}_1^0}$. This graph is very different from the corresponding one for CMSSM-ISS. In NUHM2-ISS scenario, because of low μ values, the chargino can be Higgsino-like, which yields bino-Higgsino mixed dark matter. This type of solution can be seen along the solid back line. In those cases where μ is heavy, the chargino will be wino-like as in the CMSSM-ISS case. Such solutions can be displayed in the second strip in the graph. We also display a plot in the $m_{\tilde{\chi}_1^0} - m_{\tilde{\nu}_3}$ plane where we show a minimum value $m_{\tilde{\nu}_3} \approx 250$ GeV, which is also consistent with the results reported in Ref. [41].

In Figure 10 we show graphs in $m_{\tilde{q}} - m_{\tilde{g}}$ and $m_{\tilde{\chi}_1^\pm} - m_{\tilde{l}}$ planes. In the left panel, the orange points do not satisfy the mass bounds for gluinos and first two generation squarks. The color coding otherwise is the same as in the previous figures. Dashed vertical and horizontal lines display the current squark and gluino mass bounds.

Comparing results from Figures 10 and 7, we see very small changes on the lower mass bounds for the first two generation squarks, and sleptons as well as gluinos, which is what we expected. But there are many more red points in Figure 10, because in the NUHM2-ISS case, we have the additional A -resonance and bino-Higgsino dark matter solutions for the LSP neutralino relic abundance. As in the CMSSM-ISS case, we can have squarks and gluinos in a mass range which can be explored at LHC14.

In Table 2 we present five benchmark points for NUHM2-ISS case which satisfy the phenomenological constraints discussed in section 3. Points 1, 2, 3, 4 and 5 are chosen, respectively, from the stau-neutralino coannihilation region, the bino-Higgsino mixed dark matter region, the A -resonance region, the sneutrino-neutralino coannihilation region, and the stop-neutralino

	Point 1	Point 2	Point 3	Point 4	Point 5
m_0	2452.3	1742.2	1573.4	1301.9	3116
$M_{1/2}$	1333.4	1292.1	968.18	1293.1	857.6
A_0/m_0	-2.62	-2.49	-2.60	-2.82	-2.87
$\tan \beta$	53.42	12.54	26.25	22.67	18.89
m_{H_d}	4.5484	855.55	1.8117	1.7413	737.7
m_{H_u}	2.0939	3783.2	2661.3	3060.1	3972
m_h	125	125	125	125	126
m_H	1865	1253	882	658	2782
m_A	1853	1245	876	654	2765
m_{H^\pm}	1867	1256	886	664	2784
μ	3483	6455	1448	1006	3149
$m_{\tilde{g}}$	2971	2842	2188	2816	2054
$m_{\tilde{\chi}_{1,2}^0}$	600 , 1139	556 , 656	423 , 805	563 , 979	388 , 748
$m_{\tilde{\chi}_{3,4}^0}$	3447, 3448	657 , 1080	1445, 1450	1015, 1103	314, 314
$m_{\tilde{\chi}_{1,2}^\pm}$	1141, 3448	659, 1070	807, 1451	987, 1097	755, 3151
$m_{\tilde{u}_{L,R}}$	3565, 3492	3052, 3063	2479, 2483	2836, 2815	3515, 3576
$m_{\tilde{t}_{1,2}}$	2195, 2687	1180, 2302	1078, 1819	1374, 2185	428 , 2303
$m_{\tilde{d}_{L,R}}$	3566, 3484	3053, 2943	2481, 2406	2837, 2720	3516, 3470
$m_{\tilde{b}_{1,2}}$	2628, 2776	2305, 2849	1804, 2153	2171, 2520	2329, 3160
$m_{\tilde{\nu}_1}$	2605	2021	1748	1627	3225
$m_{\tilde{\nu}_3}$	1503	804	818	568	1808
$m_{\tilde{e}_{L,R}}$	2606, 2502	2022, 1611	1749, 1502	1630, 1210	3222, 3012
$m_{\tilde{\tau}_{1,2}}$	628 , 1501	824, 1536	824, 1201	588, 972	1823, 2693
$\sigma_{SI}(\text{pb})$	1.80×10^{-12}	6.83×10^{-9}	5.11×10^{-11}	5.07×10^{-10}	2.35×10^{-13}
$\sigma_{SD}(\text{pb})$	3.80×10^{-11}	1.00×10^{-5}	2.26×10^{-8}	2.56×10^{-7}	2.1×10^{-10}
$\Omega_{CDM} h^2$	0.108	0.093	0.113	0.103	0.122

Table 2: Masses (in GeV units) and other parameters for NUHM2-ISS benchmark points satisfying all phenomenological constraints discussed in section 3. Points 1-5 are chosen, respectively, from the stau-neutralino coannihilation, the bino-Higgsino mixed dark matter, the A-resonance, the sneutrino-neutralino coannihilation, and the stop-neutralino coannihilation regions.

coannihilation region. In all the five benchmark points the first two generation squarks are in the mass range 2.4-3.5 TeV, while the first two generation sleptons lie around 1.6-3 TeV. Note that for the bino-Higgsino mixed dark matter point the spin independent cross section is 6.83×10^{-9} pb, which is below the current XENON100 bounds [42], but within the reach of XENON1T [43] and SuperCDMS [44].

5 Conclusions

The recent discovery at the LHC of a SM-like Higgs boson with mass $m_h \simeq 125$ GeV puts considerable stress on the MSSM. With $m_h \lesssim M_Z$ at tree level, large radiative corrections are required. Such corrections can be achieved in the MSSM either with multi-TeV stops, or with a large stop trilinear coupling and stop masses around 1 TeV. In models with universal sfermion masses at M_{GUT} , such as CMSSM and NUHM2, this leads to heavy sleptons and 1st/2nd generation squarks which are near or beyond the ultimate LHC reach. Various MSSM extensions have been proposed to allow lighter sfermions via additional contributions to the lightest CP-even Higgs boson mass. In this paper we explored the impact of the inverse seesaw mechanism on the sparticle mass spectrum.

The ISS mechanism allows an increase of m_h by a few GeV, while simultaneously generating mass for neutrinos via dimension six operators. With a maximal value of the Dirac Yukawa coupling involving the up-type Higgs doublet, m_h is increased by 2-3 GeV. As we have shown, this effect allows one to have lighter colored sparticles in CMSSM and NUHM2 scenarios which can be tested at LHC14. For example, in CMSSM-ISS the minimal value of m_0 is ~ 400 GeV, compared to CMSSM where $m_0 \gtrsim 800$ GeV. Furthermore, requiring neutralino LSP to be the cold dark matter (CDM) pushes m_0 to 10-20 TeV range in CMSSM, whereas in CMSSM-ISS values as low as ~ 200 GeV are allowed. This means that squarks and gluinos in CMSSM-ISS lie within the reach of LHC14. Similarly, in NUHM2-ISS squarks and gluinos in 1.5-3 TeV range are consistent with neutralino CDM. We have presented several LHC testable benchmark points with the desired neutralino dark matter relic abundance.

Acknowledgments

We would like to thank Adeel Ajaib and Cem Salih Un for useful discussions. This work is supported in part by DOE Grant No. DE-FG02-12ER41808 (I. G., B. H., and Q. S.). A. M. is also supported by a DOE grant. This work used the Extreme Science and Engineering Discovery Environment (XSEDE), which is supported by the National Science Foundation grant number OCI-1053575. I. G. acknowledges support from the Rustaveli National Science Foundation No. 03/79. B. H. would like to thank the Center for High Energy Physics at Peking University where part of this work was done for hospitality.

References

- [1] G. Aad *et al.* [ATLAS Collaboration], Phys. Lett. B **716**, 1 (2012).
- [2] S. Chatrchyan *et al.* [CMS Collaboration], Phys. Lett. B **716**, 30 (2012).
- [3] M. S. Carena and H. E. Haber, Prog. Part. Nucl. Phys. **50**, 63 (2003) and references therein.
- [4] For a review see A. Djouadi, Phys. Rept. **459**, 1 (2008) and reference therein.

- [5] I. Gogoladze, Q. Shafi and C. S. Un, JHEP **1208**, 028 (2012); N. Karagiannakis, G. Lazarides and C. Pallis, J. Phys. Conf. Ser. **384**, 012012 (2012); A. Anandakrishnan and S. Raby, Phys. Rev. Lett. **111**, 211801 (2013); M. Adeel Ajaib, I. Gogoladze, Q. Shafi and C. S. Un, JHEP **1307**, 139 (2013); M. Badziak, M. Olechowski and S. Pokorski, JHEP **10**, 088 (2013).
- [6] M. A. Ajaib, I. Gogoladze, F. Nasir and Q. Shafi, Phys. Lett. B **713**, 462 (2012).
- [7] H. Baer, V. Barger, P. Huang and A. Mustafayev, Phys. Rev. D **84** (2011) 091701; H. Baer, V. Barger and A. Mustafayev, Phys. Rev. D **85**, 075010 (2012); A. Arbey, M. Battaglia, A. Djouadi, F. Mahmoudi and J. Quevillon, *Phys. Lett. B* **708** (2012) 162; M. Carena, S. Gori, N. R. Shah and C. E. M. Wagner, *J. High Energy Phys.* **1203** (2012) 014; S. Akula, B. Altunkaynak, D. Feldman, P. Nath and G. Peim, *Phys. Rev. D* **85** (2012) 075001; M. Kadastik, K. Kannike, A. Racioppi and M. Raidal, *J. High Energy Phys.* **1205** (2012) 061; O. Buchmueller, R. Cavanaugh, A. De Roeck, M. J. Dolan, J. R. Ellis, H. Flacher, S. Heinemeyer and G. Isidori *et al.*, *Eur. Phys. J. C* **72** (2012) 2020; J. Cao, Z. Heng, D. Li and J. M. Yang, *Phys. Lett. B* **710** (2012) 665; K. A. Olive, *J. Phys. Conf. Ser.* **384** (2012) 012010; L. Roszkowski, E. M. Sessolo and Y. L. Tsai, Phys. Rev. D **86**, 095005 (2012).
- [8] A. H. Chamseddine, R. L. Arnowitt and P. Nath, Phys. Rev. Lett. **49**, 970 (1982); R. Barbieri, S. Ferrara, and C. A. Savoy, Phys. Lett. B **119**, 343 (1982); L. J. Hall, J. D. Lykken, and S. Weinberg, Phys. Rev. D **27**, 2359 (1983); E. Cremmer, P. Fayet, and L. Girardello, Phys. Lett. B **122**, 41 (1983); N. Ohta, Prog. Theor. Phys. **70**, 542 (1983).
- [9] G. Aad *et al.* [ATLAS Collaboration], Phys. Rev. D **87**, 012008 (2013).
- [10] S. Chatrchyan *et al.* [CMS Collaboration], JHEP **1210**, 018 (2012).
- [11] CMS Collaborations, CMS NOTE -2012/006
- [12] M. C. Gonzalez-Garcia, M. Maltoni, J. Salvado and T. Schwetz, JHEP **1212**, 123 (2012).
- [13] R. N. Mohapatra *et al.*, Rept. Prog. Phys. **70**, 1757 (2007) [hep-ph/0510213].
- [14] R. N. Mohapatra, Phys. Rev. Lett. **56**, 561 (1986); R. N. Mohapatra and J. W. F. Valle, Phys. Rev. D **34**, 1642 (1986).
- [15] I. Gogoladze, N. Okada and Q. Shafi, Phys. Lett. B **672**, 235 (2009) [arXiv:0809.0703 [hep-ph]]; I. Gogoladze, B. He and Q. Shafi, Phys. Lett. B **718**, 1008 (2013) [arXiv:1209.5984 [hep-ph]].
- [16] J. Guo, Z. Kang, T. Li and Y. Liu, arXiv:1311.3497 [hep-ph].
- [17] J. Ellis, K. Olive and Y. Santoso, *Phys. Lett. B* **539** (2002) 107; J. Ellis, T. Falk, K. Olive and Y. Santoso, *Nucl. Phys. B* **652** (2003) 259; H. Baer, A. Mustafayev, S. Profumo, A. Belyaev and X. Tata, *J. High Energy Phys.* **0507** (2005) 065.

- [18] P. S. B. Dev and R. N. Mohapatra, Phys. Rev. D **81**, 013001 (2010); S. Khalil, Phys. Rev. D **82**, 077702 (2010). Z. Kang, J. Li, T. Li, T. Liu and J. Yang, arXiv:1102.5644 [hep-ph]; S. Khalil, H. Okada and T. Toma, JHEP **1107**, 026 (2011); F. -X. Josse-Michaux and E. Molinaro, Phys. Rev. D **84**, 125021 (2011); H. An, P. S. B. Dev, Y. Cai and R. N. Mohapatra, Phys. Rev. Lett. **108**, 081806 (2012); P. S. Bhupal Dev, S. Mondal, B. Mukhopadhyaya and S. Roy, JHEP **1209** (2012) 110; L. Basso, O. Fischer and J. J. van der Bij, Phys. Rev. D **87**, no. 3, 035015 (2013); S. Banerjee, P. S. B. Dev, S. Mondal, B. Mukhopadhyaya and S. Roy, JHEP **1310**, 221 (2013).
- [19] K. S. Babu, I. Gogoladze, M. U. Rehman and Q. Shafi, Phys. Rev. D **78**, 055017 (2008); S. P. Martin, Phys. Rev. D **81**, 035004 (2010) [arXiv:0910.2732 [hep-ph]].
- [20] H. Baer, F. E. Paige, S. D. Protopopescu and X. Tata, hep-ph/0001086.
- [21] [Tevatron Electroweak Working Group and CDF Collaboration and D0 Collab], arXiv:0903.2503 [hep-ex].
- [22] J. Beringer *et al.* [Particle Data Group Collaboration], Phys. Rev. D **86**, 010001 (2012).
- [23] H. Baer and M. Brhlik, *Phys. Rev. D* **55** (1997) 4463; H. Baer, M. Brhlik, D. Castano and X. Tata, *Phys. Rev. D* **58** (1998) 015007.
- [24] D. Eriksson, F. Mahmoudi and O. Stal, *J. High Energy Phys.* **0811** (2008) 035.
- [25] G. Aad *et al.* [ATLAS Collaboration], Phys. Lett. B **716**, 1 (2012).
- [26] S. Chatrchyan *et al.* [CMS Collaboration], Phys. Lett. B **716**, 30 (2012) and arXiv:1303.4571 [hep-ex].
- [27] R. Aaij *et al.* [LHCb Collaboration], Phys. Rev. Lett. **110**, 021801 (2013).
- [28] Y. Amhis *et al.* [Heavy Flavor Averaging Group Collaboration], arXiv:1207.1158 [hep-ex].
- [29] D. Asner *et al.* [Heavy Flavor Averaging Group Collaboration], arXiv:1010.1589 [hep-ex].
- [30] G. Hinshaw *et al.* [WMAP Collaboration], arXiv:1212.5226 [astro-ph.CO].
- [31] J. L. Feng, K. T. Matchev and T. Moroi, Phys. Rev. Lett. **84**, 2322 (2000) and Phys. Rev. D **61**, 075005 (2000); J. L. Feng, K. T. Matchev and F. Wilczek, Phys. Lett. B **482**, 388 (2000).
- [32] K. L. Chan, U. Chattopadhyay and P. Nath, Phys. Rev. D **58**, 096004 (1998).
- [33] H. Baer, I. Gogoladze, A. Mustafayev, S. Raza and Q. Shafi, JHEP **1203**, 047 (2012).
- [34] I. Gogoladze, S. Raza and Q. Shafi, Phys. Lett. B **706**, 345 (2012).
- [35] M. A. Ajaib, T. Li and Q. Shafi, Phys. Rev. D **85**, 055021 (2012).
- [36] B. He, T. Li and Q. Shafi, JHEP **1205**, 148 (2012).

- [37] M. Drees and M. M. Nojiri, Phys. Rev. D **47** (1993) 376; H. Baer and M. Brhlik, Phys. Rev. D **53** (1996) 597 and Phys. Rev. D **57** (1998) 567; H. Baer, M. Brhlik, M. A. Diaz, J. Ferrandis, P. Mercadante, P. Quintana and X. Tata, Phys. Rev. D **63** (2001) 015007; A. B. Lahanas, D. V. Nanopoulos and V. C. Spanos, Mod. Phys. Lett. A **16** (2001) 1229; A. B. Lahanas and V. C. Spanos, Eur. Phys. J. C **23** (2002) 185.
- [38] J. R. Ellis, T. Falk and K. A. Olive, Phys. Lett. B **444** (1998) 367; J. R. Ellis, T. Falk, K. A. Olive and M. Srednicki, Astropart. Phys. **13** (2000) 181 [Erratum-ibid. **15** (2001) 413]; R. Arnowitt, B. Dutta and Y. Santoso, Nucl. Phys. B **606** (2001) 59; M. E. Gómez, G. Lazarides and C. Pallis, Phys. Rev. D **D61** (2000) 123512; Phys. Lett. **B487** (2000) 313; Nucl. Phys. B **B638** (2002) 165; T. Nihei, L. Roszkowski and R. Ruiz de Austri, JHEP **0207** (2002) 024.
- [39] C. Boehm, A. Djouadi and M. Drees, Phys. Rev. D **62**, 035012 (2000); J. R. Ellis, K. A. Olive and Y. Santoso, Astropart. Phys. **18**, 395 (2003); J. Edsjo, M. Schelke, P. Ullio and P. Gondolo, JCAP **0304**, 001 (2003); J. L. Diaz-Cruz, J. R. Ellis, K. A. Olive and Y. Santoso, JHEP **0705**, 003 (2007).
- [40] H. Baer, V. Barger, P. Huang, D. Mickelson, A. Mustafayev and X. Tata, Phys. Rev. D **87**, no. 3, 035017 (2013); I. Gogoladze, F. Nasir and Q. Shafi, Int. J. Mod. Phys. A **28**, 1350046 (2013).
- [41] N. Okada, S. Raza and Q. Shafi, arXiv:1307.0461 [hep-ph].
- [42] E. Aprile *et al.* [XENON100 Collaboration], Phys. Rev. Lett. **109**, 181301 (2012).
- [43] The XENON Dark Matter Project
http://xenon.astro.columbia.edu/talks/aprile_ucla_dm2010.pdf/
- [44] http://cdms.berkeley.edu/APS_Panofsky_130413_Cabrera.pdf/